RSC Advances

PAPER

View Article Online
View Journal | View Issue



Cite this: *RSC Adv.*, 2025, **15**, 101

# Exploration of novel triazolo-thiadiazine hybrids of deferasirox as multi-target-directed anti-neuroinflammatory agents with structure–activity relationship (SAR): a new treatment opportunity for Alzheimer's disease†

Syed Ahmed Shakir,[a] Umer Rashid, *[a] Marryum,[a] Nighat Fatima,[b] Syeda Abida Ejaz,[c] Ammara Fayyaz,[c] Muhammad Zahid Ullah,[a] Aamer Saeed, [d] Ajmal Khan,[ef] Ahmed Al Harrasi [e] and Amara Mumtaz *[a]

It is believed that inflammation influences several physiological processes, including the function of the central nervous system. Moreover, the impairment of lipid mechanisms/pathways is associated with neurodegenerative disorders and onset of Alzheimer's disease (AD). AD is a chronic neurodegenerative disease representing the major cause of dementia worldwide. In this case, the overexpression of different pharmacological targets has been confirmed to address neuronal inflammation and AD, with acetylcholinesterase (AChE), monoamine oxidase-B (MAO-B), cyclooxygenase-2 (COX-2) and 5-lipoxygenase (LOX-5) being the most explored targets. Currently, the available treatments are only capable of alleviating the symptoms and not capable of delivering disease-modifying effects. Thus, the current research objective is to synthesize triazolo-thiadiazine derivatives of the deferasirox drug as multi-target compounds that could concurrently inhibit ChEs, MAOs, LOX-5 and COX-2. The synthesized derivatives were confirmed by FTIR, $^{1}$H NMR, $^{13}$C NMR and DEPT-135 spectroscopic techniques. During *in vitro* investigations, compound **11** was found to be the most potent inhibitor of all the targeted enzymes. Briefly, this compound exhibited inhibitory values ($IC_{50} \pm SEM$) of 0.31 ± 0.16, 0.13 ± 0.16 and 0.94 ± 0.16 μM against AChE, MAO-B and COX-2, respectively, suggesting that it is a lead molecule for the synthesis of more potential multi-targeted inhibitors. Several compounds, such as compound **9** and **13**, showed dual inhibition potential in comparison to standard drugs. Furthermore, molecular docking analysis was performed to validate the *in vitro* results, where the potent compounds showed some significant interactions with the key amino acids present in the active site of the targeted enzymes. Furthermore, molecular dynamics (MD) simulation data and physicochemical properties supported deferasirox-substituted triazolo-thiadiazine as a promising horizon for the discovery and development of new molecules to treat multifactorial diseases associated with neuro-inflammation, such as AD.

Received 25th September 2024
Accepted 25th November 2024

DOI: 10.1039/d4ra06916a

rsc.li/rsc-advances

## 1 Introduction

Cognitive dysfunctions, such as low information processing speed, deficits in learning, persistent attention-deficit dysfunctions, poor visual perception, low mental flexibility, and memory loss, are the major symptoms of Alzheimer's disease (AD).[1] In this case, acetylcholine (ACh) helps in regulating cognitive functions, particularly memory and learning, *via* neurotransmission. Acetyl co-enzyme A, along with choline, is the primary source for ACh synthesis in presynaptic neurons, from where Ach is released into the synaptic gaps.[2] Acetylcholinesterase (AChE) disrupts ACh-mediated neurotransmission, which initially originates in neurons. AChE inhibitors are administered in AD therapy as they have the ability to increase

[a]*Department of Chemistry, COMSATS University Islamabad, Abbottabad Campus, 22060, Pakistan. E-mail: umerrashid@cuiatd.edu.pk; amaramumtaz@cuiatd.edu.pk; Tel: +923334517999; +923005316570*

[b]*Department of Pharmacy, COMSATS University Islamabad, Abbottabad Campus, 22060, Pakistan*

[c]*Department of Pharmaceutical Chemistry, Faculty of Pharmacy, The Islamia University of Bahawalpur, Bahawalpur 63100, Pakistan*

[d]*Department of Chemistry, Quaid-i-Azam University, Islamabad, 45320, Pakistan*

[e]*Natural and Medical Sciences Research Center, University of Nizwa, 616, Nizwa, Oman*

[f]*Department of Chemical and Biological Engineering, College of Engineering, Korea University, 145 Anan-RO, Seongbuk-Gu, Seoul, 02841, Korea*

† Electronic supplementary information (ESI) available. See DOI: https://doi.org/10.1039/d4ra06916a

synaptic ACh levels in the cerebral cortex and recover cholinergic transmission.[3] AD is associated with a reduction in the Ach level, leading to central nervous system (CNS) disorders and, consequently, a gradual decline in cognitive function, memory, and cognition.[4] At present, FDA-approved AChE inhibitors for the treatment of AD are galantamine, rivastigmine and donepezil.[5] Similar to AChE, butyrylcholinesterase (BChE) significantly contributes to cholinergic neurotransmission. BChE is present in the hippocampus, temporal nerve cortex, and glial cells and is associated with cognitive function.[6] In comparison to AChE, BChE has lesser substrate specificity, but both enzymes effectively hydrolyze AChE.[7] In contrast, monoamine oxidases (MAOs) are considered responsible for the inactivation of catecholamine and 5-hydroxytryptamine, and therefore, they are targeted in diseases where they are considered to be involved. Additionally, selective MAO-A inhibitors possess antidepressant activity. Thus, selective MAO-B inhibitors are employed as progressive targets for the treatment of AD and Parkinson's disease (PD).[8]

Although the key roots of neurodegenerative diseases are diverse, microglial activation and neuroinflammation are common features in most of these diseases and the adoption of anti-inflammatory approaches to avoid neurodegeneration has been studied intensively and endorsed as a promising approach.[9] Consequently, COX-1 and COX-2 have attracted significant attention, and their inhibitors are considered neuroprotective in different settings of neurotoxicity and neurodegeneration.[10] COX-2 inhibitors have been uncovered as neuroprotective in several ischemia models, as well as *in vitro* and *in vivo* models of diseases such as Alzheimer's, Parkinson's and amyotrophic lateral sclerosis.[11] Similarly, significant results show that 5-lipoxygenase (5-LOX), a proinflammatory protein enzyme, is a prominent modulator in the onset of age-related neuropathology. It is further believed that age-related brain diseases can be delayed or slowed down just by the inhibition of 5-LOX activation.[12]

Triazolo-thiadiazines are a class of compounds formed by the fusion of two active pharmacophore moieties, *i.e.*, triazole and thiadiazine. Triazolo-thiadiazines have been found to have promising activity against different targets such as anticancer, antimicrobial,[13] anti-Alzheimer's, anti-and inflammatory.[14] Triazolothiadiazines show specific interactions with many different receptors due to their hydrogen bond-accepting and donating capability, making them significant pharmacophores with excellent bioactive profiles.[15] Triazolothiadiazines can be synthesized by condensing the triazole amine with substituted phenacyl bromides in absolute ethanol.[16] Here, we present some of the reported triazolo-thiadiazine derivatives possessing cholinesterase and monoamine oxidase inhibition potential[17–19] (Fig. 1).

The multi-target-directed ligand (MTDL) strategy is an effective method for discovering novel medications because of

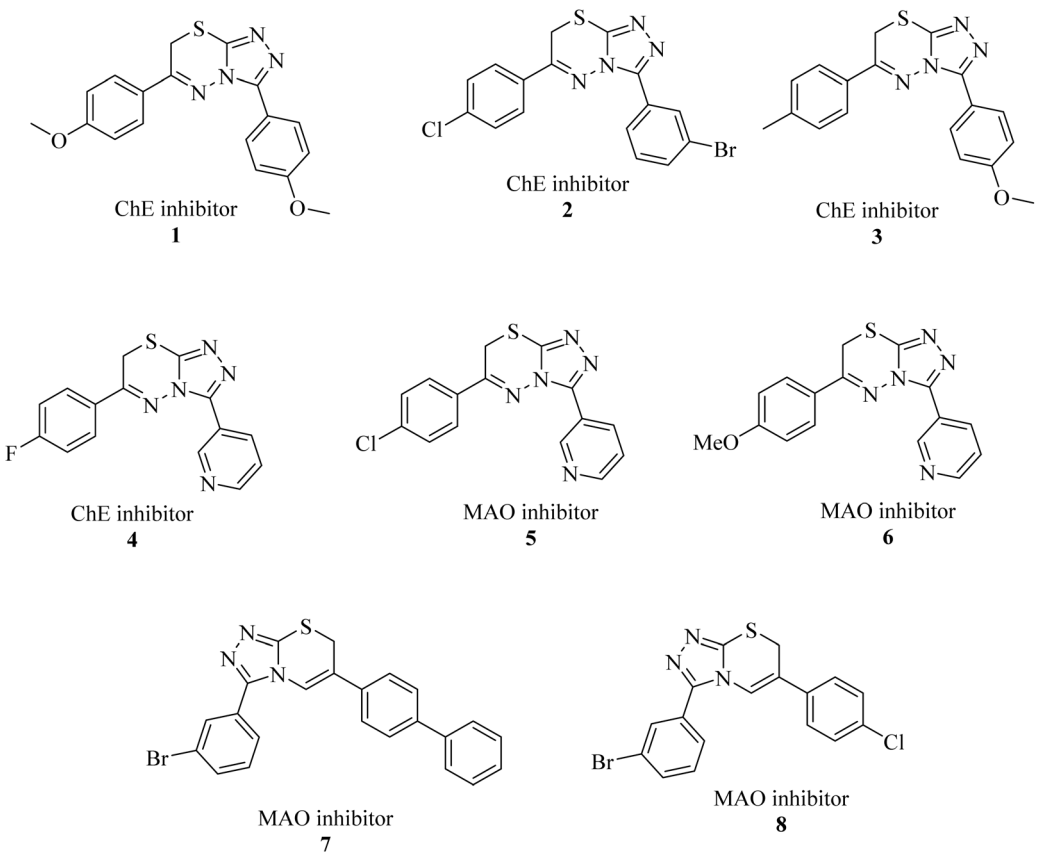


Fig. 1 Previously reported triazolo-thiadiazine derivatives as cholinesterase and monoamine oxidase inhibitors.[17–19]

the complex nature of the causes of AD.[20] In the field of contemporary drug development, the MTDL technique has gained considerable interest and is emerging as a viable therapy option for the intricate AD. This strategy involves the fusion of more than two biologically active pharmacophores into a single molecule. Most of the newly identified diverse multitarget-directed ligands (MTDLs) function as inhibitors for many enzymes, such as acetylcholinesterase (AChE), monoamine oxidase (MAO), beta-secretase 1 (BACE1), and phosphodiesterase 4D (PDE4D). Furthermore, MTDLs that target AD exhibit the characteristics of regulators of serotonin receptors (5-HT), metal chelators, antiaggregant, neuroprotective and antioxidants agents.[15,17–19] Herein, we presents a thorough evaluation of the recently discovered deferasirox derivative drugs that can interact with many targets by utilizing a mix of several pharmacophores for Alzheimer's treatment. These inhibitors have the potential to be effective therapies for AD.

# 2 Results and discussion

## 2.1. Instrumentation

Melting points were recorded in capillary tubes using an electrothermal melting point instrument, model Stuart digital melting point (SMP 10) apparatus with the specification of OE\Digital (08-09), 169/1 DMPA, 09-01. $^1$H NMR and $^{13}$C NMR spectra were recorded on a Bruker Avance III HD 400, 100 MHz spectrometer at the Department of Chemistry, COMSATS University Islamabad, Abbottabad Campus and Bruker 600, 150 MHz spectrometer at the Natural and Medical Sciences Research Center, University of Nizwa, respectively, utilizing DMSO-$d_6$ (deuterated) as the solvent and TMS (tetramethylsilane) as the internal reference. High-resolution electrospray ionization mass spectra (HR-ESI-MS) were recorded on an Agilent 6530 LCQ-ToF instrument.

## 2.2. Chemistry

The synthesis of deferasirox-substituted triazole amine **13** was carried out by using the following steps, as reported in Scheme 1.[21] The first deferasirox derivative **10** was synthesised by refluxing the drug in excess methanol in the presence of sulfuric acid as a catalyst. The structure of **10** was confirmed by $^1$H-NMR. In the $^1$H-NMR analysis, the appearance of characteristic signals at 3.86 ppm as a singlet for 3 methoxy protons, in addition to the deferasirox signals confirmed the formation of an ester. Subsequently, ester **10** was reacted with hydrazine monohydrate in excess, in a methanolic solution to acquire the hydrazide derivative of deferasirox **11**, whose structure was confirmed by $^1$H NMR with the disappearance of the methoxy signal of ester and appearance of two broad signals of NH and NHCO groups at 4.55 and 10.08, respectively. **11** was converted to compound **13** by first converting to derivative and intermediate deferasirox-substituted oxadiazole **12**. The synthesis of oxadiazole derivative **12** was carried out by refluxing **11** with $CS_2$ and KOH in ethanol for 12–15 h, and then the white precipitate obtained were washed with diethyl ether, and upon refluxing with the

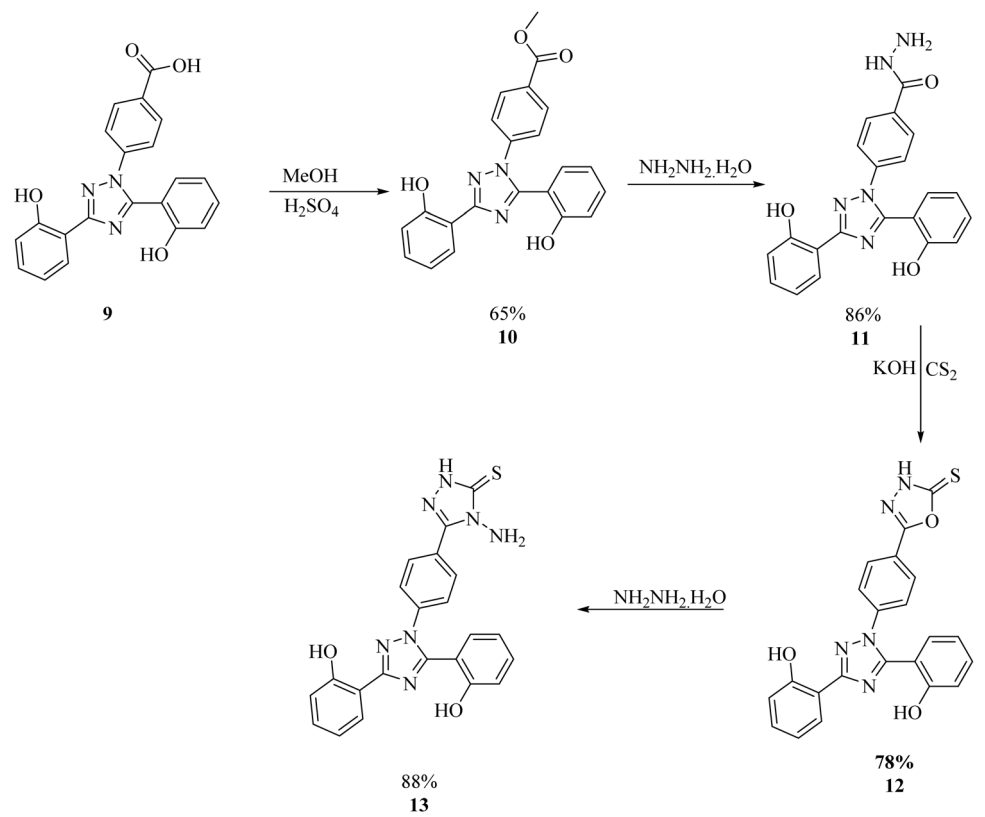


Scheme 1 General procedure for the synthesis of the 1,3,4-triazole amine.[21]

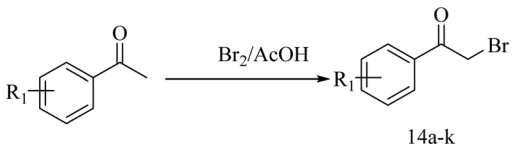


14a-k

14a: $R_1$ = 4-Cl-Ph, (78%)
14b: $R_1$ = 3-$NO_2$-Ph (81%)
14c: $R_1$ = 4-CN-Ph (56%)
14d: $R_1$ = Phenyl (78%)
14e: $R_1$ = 4-OMe-Ph, (88%)
14f: $R_1$ = 2-OH-Ph, (77%)
14g: $R_1$ = 4-$SCH_3$-Ph (54%)
14h: $R_1$ = Naphthyl coumarin, (83%)
14i: $R_1$ = 5-bromo coumarin, (88%)
14j: $R_1$ = 4-OH-Ph, (72%)
14k: $R_1$ = 2,6-$Cl_2$-Ph, (77%)

Scheme 2 General procedure for the synthesis of α-bromoacetophenones.

hydrochloric acid compound, **13** was obtained in good yield. The structure of compound **13** was confirmed by $^1$H NMR and $^{13}$C NMR.[21] The $^1$H NMR data confirmed the formation of a ring after the appearance of two characteristic signals at 14.02 and 5.80 ppm for the NH and $NH_2$ groups, respectively. The $^{13}$C NMR data further supported this data with the appearance of signals at 167.3 and at 156.8 ppm supporting ring closure[21] (Scheme 1). The physical data of compounds **10–13** is presented in Table S1.†

For the synthesis of the deferasirox-substituted triazolo-thiadiazine derivatives (**15–25**), α-bromoacetophenones (**14a–k**) were synthesised *via* the reaction of substituted acetophenones with bromine in acetic acid (Scheme 2), respectively. The synthesis of the α-bromoacetophenones was confirmed by their melting points and comparison with the literature. Table S2† shows the details of the synthesized α-bromoacetophenones and their melting points (Scheme 2).

Our targeted compounds, triazolo-thiadiazine derivatives of deferasirox (**15–25**), were synthesized *via* the condensation of an alcoholic solution of triazole amine (**13**) with the substituted alpha bromo-acetophenones (**14a–k**) in the presence of potassium carbonate. Our targeted molecules were obtained in a good yield ranging from 65–88% (Table S3†). Structural confirmation was carried out based on the disappearance of the $NH_2$ singlet of triazole amine derivative **13** and appearance of a characteristic singlet at 4.42–4.55 ppm for the $CH_2$ group of triazolo-thiadiazine, confirming the ring closure. Further confirmation was carried out by $^{13}$C NMR analysis. In the $^{13}$C NMR spectra, the appearance of the characteristic signal of the $CH_2$ group at 23.2–23.4 ppm confirmed the ring closure. DEPT-135 further confirmed the ring closure with the appearance of an inverted signal for the $CH_2$ group in the same region (Scheme 3).

### 2.3. Biological activities

**2.3.1 *In vitro* cholinesterase inhibition assay.** The deferasirox-substituted derivatives (**10–13** and **15–25**) were tested against both cholinesterase (AChE and BChE) enzymes using Ellman's method.[22] Donepezil was used as a control. Compounds **9**, **10**, **11** and **13** showed significant inhibition of AChE. Among these compounds, **11** showed more potential than the other derivatives with an $IC_{50}$ value of 0.31 ± 0.02 μM and found to be less potent in comparison to donepezil, which has inhibition potential of 0.047 ± 0.001 μM (Table 1). The other triazolothiadiazine derivatives, *i.e.*, **15–25**, showed no activity against AChE. Generally, all the derivatives showed good activity against BChE compared to AChE. The inhibitory activity against BChE varied considerably. Compounds **9**, **11**, **13**, **16**, **20** and **23** displayed excellent to moderate activity, among which compound **11** showed excellent inhibition with an $IC_{50}$ value of 0.094 ± 0.001 μM, while **17** (0.28 ± 0.03 μM), **19** (0.13 ± 0.02 μM), **22** (10.84 ± 0.97 μM), **24** (0.17 ± 0.02 μM), and **25** (0.81 ± 0.02 μM) showed moderate activity.

**2.3.2 *In vitro* MAO-A and MAO-B inhibition assay.** All the compounds were tested for their MAO-A and MAO-B inhibition potential. Safinamide was used as a reference control, which exhibited inhibition potency of 6.71 ± 0.76 μM and 0.0027 ±

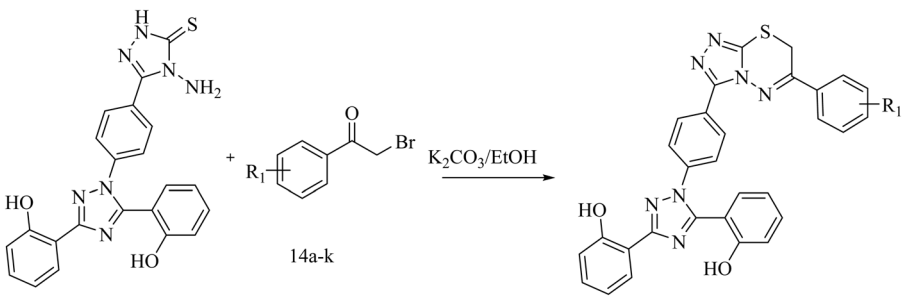


15: $R_1$ = 4-Cl-Ph, (81%)
16: $R_1$ = 3-$NO_2$-Ph, (85%)
17: $R_1$ = 4-CN-Ph, (68%)
18: $R_1$ = Phenyl-Ph, (73%)
19: $R_1$ = 4-OMe-Ph, (67%)
20: $R_1$ = 2-OH-Ph, (63%)
21: $R_1$ = 4-$SCH_3$-Ph, (77%)
22: $R_1$ = Naphthyl coumarin, (88%)
23: $R_1$ = 5-bromo coumarin, (65%)
24: $R_1$ = 4-OH-Ph, (88%)
25: $R_1$ = 2,6-$Cl_2$-Ph, (78%)

Scheme 3 General procedure for the synthesis of triazolo-thiadiazine (**15–25**).

Table 1 Inhibitory effects of the synthesized derivatives (**9–13** and **15–25**) against various targets

| | | $IC_{50}$ (μM) ± SEM | | | | | |
|---|---|---|---|---|---|---|---|
| Code | Structure | AChE | BChE | MAO-A | MAO-B | COX-2 | 5-LOX |
| **09** | 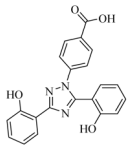 | 0.43 ± 0.05 | 0.11 ± 0.005 | 10.05 ± 1.78 | 0.18 ± 0.01 | 4.93 ± 0.38 | 1.28 ± 0.13 |
| **10** | 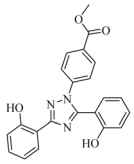 | 6.24 ± 0.16 | 0.45 ± 0.02 | 33.59 ± 3.09 | 19.55 ± 1.94 | 1.12 ± 0.14 | 26.94 ± 3.54 |
| **11** | 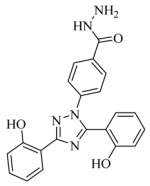 | 0.31 ± 0.02 | 0.094 ± 0.001 | 10.15 ± 1.21 | 0.13 ± 0.02 | 0.94 ± 0.11 | 12.73 ± 2.09 |
| **13** | 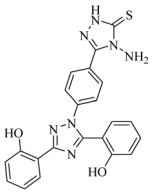 | 0.71 ± 0.16 | 0.18 ± 0.02 | 19.04 ± 2.44 | 0.41 ± 0.04 | 0.07 ± 0.001 | 0.84 ± 0.05 |
| **15** | 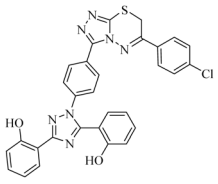 | n.a | 3.96 ± 0.22 | 3.58 ± 0.56 | n.a | 75.29 ± 3.56 | n.a |
| **16** | 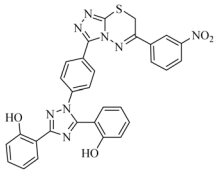 | n.a | 6.88 ± 0.39 | 6.67 ± 0.78 | n.a | 79.55 ± 3.09 | na |
| **17** | 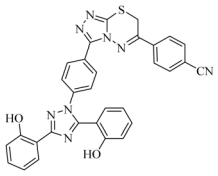 | n.a | 0.28 ± 0.03 | 55.91 ± 5.08 | n.a | n.a | na |
| **18** | 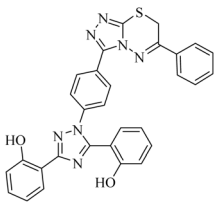 | n.a | 3.66 ± 0.89 | 0.63 ± 0.01 | n.a | n.a | na |

Table 1 (*Contd.*)

| Code | Structure | $IC_{50}$ (μM) ± SEM | | | | | |
|---|---|---|---|---|---|---|---|
| | | AChE | BChE | MAO-A | MAO-B | COX-2 | 5-LOX |
| **19** | 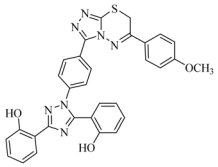 | n.a | 0.13 ± 0.02 | 2.91 ± 0.02 | n.a | n.a | na |
| **20** | 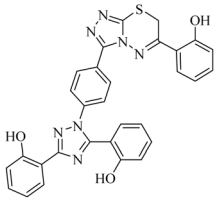 | n.a | 0.47 ± 0.05 | 4.71 ± 0.07 | n.a | n.a | na |
| **21** | 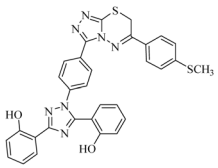 | n.a | 0.89 ± 0.06 | 1.52 ± 0.08 | n.a | n.a | n.a |
| **22** | 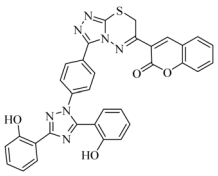 | n.a | 10.84 ± 0.97 | 0.61 ± 0.07 | n.a | n.a | n.a |
| **23** | 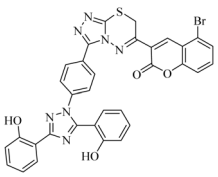 | n.a | 13.99 ± 1.11 | 1.32 ± 0.11 | n.a | n.a | n.a |
| **24** | 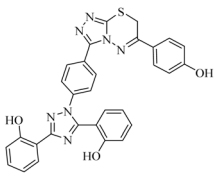 | n.a | 0.17 ± 0.02 | 23.44 ± 1.67 | n.a | n.a | n.a |
| **25** | 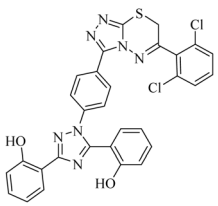 | n.a | 1.09 ± 0.11 | 0.81 ± 0.02 | n.a | n.a | n.a |
| **Donepezil** | | 0.047 ± 0.001 | 5.72 ± 0.43 | — | — | — | — |
| **Safinamide** | | — | — | 6.71 ± 0.76 | 0.027 ± 0.001 | — | — |
| **Celecoxib** | | — | — | — | — | 0.055 ± 0.002 | — |
| **Zileuton** | | — | — | — | — | — | 0.68 ± 0.009 |

0.001 μM against MAO-A and MAO-B, respectively. Interestingly, most of the hybrids showed higher inhibitory activity against MAO-A compared to MAO-B. Compounds **19**, **22** and **25** showed moderate to significant inhibition potential of 2.91 ± 0.02 μM, 0.61 ± 0.07 μM and 0.81 ± 0.02 μM, respectively, against MAO-A. Compounds **9** and **11** with the inhibition potential of 0.18 ± 0.01 μM and 0.13 ± 0.02, respectively, showed good activity against MAO-B (Table 1).

**2.3.3 *In Vitro* cyclooxygenase-2 and 5-LOX inhibition assays.** *In vitro* COX-2 and LOX-5 inhibition assays were performed according to the enzyme immune assay (EIA), as reported in literature.[23] All the synthesized compounds were tested against these enzymes using the reference controls celecoxib ($IC_{50}$ = 0.055 ± 0.002 μM) and zileuton ($IC_{50}$ = 0.68 ± 0.009 μM), respectively. Compounds **9**, **10**, **11**, **13**, **15** and **16** showed good to moderate activity against COX-2. Among them, **13** showed the greatest inhibition *i.e.*, 0.07 ± 0.001 μM, which is quite close to the reference drug celecoxib having inhibition of 0.055 ± 0.002 μM. None of the compounds showed activity against 5-LOX except for compound **13**, which was also very poor (Table 1).

**2.3.4 Structure activity relationship (SARs).** Considering the biological activities of our synthesized deferasirox-substituted triazolo-thiazole hybrids, we divided their structure into three zones for better understanding.

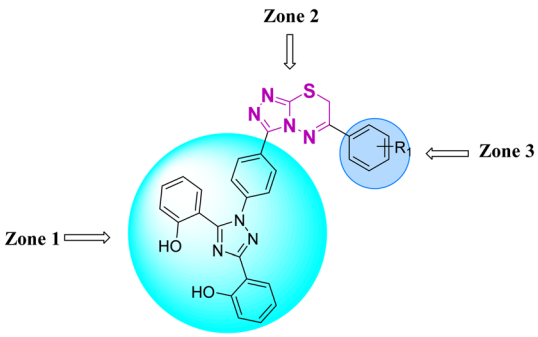


Zone 1 and zone 2 were similar in all inhibitors, while the only difference in the structures was in zone 3 due to the presence of different substituents at the aromatic ring, which are responsible for the different activities. According to the activity results shown in Table 1, the deferasirox derivatives (**10–13** and **15–25**) showed reasonable activity against different targets. Most of the compounds showed selective inhibition against different enzymes. Table 1 indicates their greater selectivity for BChE and MAO-A. Also, the activity of deferasirox was tested against all the enzymes in comparison to its derivatives.

Regarding cholinesterase, all the derivatives were tested against AChE and BChE. In case of AChE, compound **11**, a hydrazide derivative of deferasirox, showed greater inhibition potential with $IC_{50}$ values of 0.31 ± 0.02 μM, which is due to the presence of an electron-donating group (–$NH_2$). After, the activity of compound **13**, the 1,3,4-triazole-2-thione amine derivative of deferasirox, was observed, showing an $IC_{50}$ value of 0.71 ± 0.16 μM. The presence of a free $NH_2$ group and five-membered ring having three nitrogen atoms makes it the most potent derivative of in this series. In contrast, the other compounds showed no activity against AChE. In the case of BChE, the compounds exhibited poor to excellent inhibition potential and this variation in activity is due to the presence of electron-withdrawing/donating groups at different positions in zone 3. Among them, the most potent activities were observed by compound **9**, deferasirox, with an $IC_{50}$ value of 0.11 ± 0.005 μM, **11**, the hydrazide derivative, with an $IC_{50}$ value of 0.094 ± 0.001 μM, **13**, the triazoleamine derivative of deferasirox, with an $IC_{50}$ value of 0.18 ± 0.02 μM, triazolo-thiadiazine derivative **19** having a methoxy group at the *para* position of zone 3 of the phenyl group with an $IC_{50}$ value of 0.13 ± 0.02 μM and compound **24** having a hydroxy group at the *para* position of the phenyl ring in zone 3 with an $IC_{50}$ value of 0.17 ± 0.02 μM. Low activity was shown by compound **16** with an $IC_{50}$ value of 6.88 ± 0.39, compound **20** with an $IC_{50}$ value of 0.46 ± 0.05 μM and compound **23** with an $IC_{50}$ value of 13.99 ± 1.11 μM having electron-donating groups (–$NO_2$, –OH, and –Br) on *ortho* and *meta* position of the phenyl ring in zone 3, respectively. Compound **19** showed good inhibition against BChE due to the presence of an electron-withdrawing group at the *para* position. Thus, according to the activity chart, it was observed that the presence of substitution at the *para* position of the phenyl ring in zone 3 makes these compounds more potent compared to substitution at the *ortho* and *meta* positions.[24]

In the case of both monoamine oxidases A and B, the presence of a carboxylic group in compound **9** made it the most potent inhibitor. The next efficient activities were observed by compound **11**, a hydrazide derivative of deferasirox, where the presence of free $NH_2$ and amide groups was the reason for its enhanced activity against both isozymes MAO A and B. Activity against the MAO A enzyme was observed by deferasirox-substituted triazolothiadiazole derivative **19** having methoxy group at the *para* position of the phenyl ring in zone 3, **22** having a coumarinyl group in zone 3 and **25** having two chloro groups at the 2 and 6 positions of the phenyl ring in zone 3. The presence of a methoxy group, fused phenyl rings and chloro groups in zone 3 enhanced the activity of compounds **19**, **22**, and **25**.[25] The other compounds showed moderate activity against MAO-A, while no activity was observed against MAO-B for the rest of compounds.

In the case of cyclooxygenase-2 activity, compound **13**, the triazole amine derivative of deferasirox, showed good inhibition potential, while the other compounds showed moderate activity or no activity. In the case of 5-Lox, the most potent results were observed by compound **13**, the triazole amine derivative of deferasirox, and compound **11**, the hydrazide derivative of deferasirox, while the other compounds showed no activity against 5-LOX.[26]

## 2.4. Molecular docking investigations

To assess the binding affinities and inhibition profiles of the compounds within the active pocket of the targeted enzymes such as AChE, BuChE, MAO-A, MAO-B, COX-2, and LOX-5, a molecular docking analysis was conducted using the Molecular Operating Environment (MOE) software.[27] Initially the co-crystal ligands were re-docked within the active sites of the

targets to validate the docking protocol. After validation, the synthesized hybrids were allowed to dock within the active pockets of the targeted proteins. The docking poses of the compounds exhibited a similar conformation as that of the respective co-crystal ligands, validating the docking protocol, and in all cases, suitable RMSD values were observed. The crystallographic structure of the targets was obtained from the Protein Data Bank in the PDB format, specifically using the PDB accession code 1EVE for AChE,[28] 4BDS for BuChE,[29] 2Z5X for MAO-A,[30] 2V5Z for MAO-B,[31] 1CX2 for COX-2 (ref. 32) and 6N2W for 5-LOX.[33] The binding score of each compound within the active pocket of targeted enzyme is given in the Tables S4–S6.†

**2.4.1 Binding mode of compounds 9 and 13 in the binding site of AChE.** Visual inspection of the binding mode of compound **9** within the binding site of AChE revealed that the conventional hydrogen bonding is an important interaction, which explains the stability of the molecular complex. Briefly, two hydrogen bonds were formed between the GLY118 and GLY119 amino acid residues with the hydroxyl groups attached at the benzoic acid ring, and one hydrogen bond was formed between the phenol ring and PHE331, respectively. In addition, the hydrophobic interactions of compound **9** were also observed with the TYR334, PHE330 and TRP279 amino acid residues (Fig. 2a). Similarly, in compound **13**, GLU199 formed one hydrogen bond interaction with the nitrogen atom attached at the benzohydride ring and another hydrogen bond was formed between the PHE331 and phenyl ring of the compound. The amino acids that do not participate in bonding were observed as hydrophobic interactions involving the TYR334, PHE330 and HIS440 amino acid residues (Fig. 2b).

**2.4.2 Binding mode of compounds 9 and 12 in the binding site of BChE.** The active site of BChE contains the key amino acid residues that are vital for inhibition of the enzyme including HIS438 and SER198, as a catalytic triad, and also contains TYR332 and GLU325Glu325 amino acid residues (Table S4†).

The visual inspection of compound **9** within the active site of BChE revealed that the carbonyl group forms hydrogen bond interactions with the TRP82 and TRP430 amino acid residues. The two aromatic rings containing hydroxyl groups form hydrophobic interaction (pi–pi) with the GLY115, GLY116, TRP231, and PHE329 amino acid residues. The triazole ring forms hydrophobic interaction (pi–pi) with the HIS428 amino acid residue. The hydrophilic interaction with GLY117 is formed by the nitrogen atom of the triazole ring (Fig. 3a).

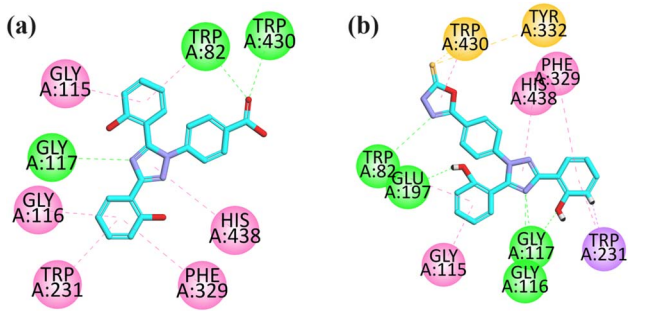


Fig. 3 2D interaction plot of compounds **9** (a) and **12** (b) in the binding site of BuChE (4BDS), modeled by using the Discovery Studio Visualizer.

The visual inspection of the binding mode of compound **12** in the binding site of BChE revealed that five hydrogen bond interactions are formed by this compound with the TRP82, GLU197, GLU117, and GLU116 amino acid residues. Three hydrophobic interactions (pi–pi) were formed by compound **12**, where two are formed between HIS438 and PHE329 with a triazole ring and one is formed between the phenyl ring and GLY115 amino acid residue. In addition, a pi–sigma interaction is also formed by an aromatic ring with TRP231 (Fig. 3b).

**2.4.3 Binding mode of compound 18 and 21 in the binding site of MAO-A.** MAO-A and MAO-B are encoded by two adjacent gene products on the X-chromosome, with different molecular weights and immunological properties. They share about 70% homology and neurons routinely contain both forms. The structure of human MAO-A (*h*-MAO-A) is composed of two domains, which are specifically the membrane binding domain and the additional membrane. It is anticipated that the additional membrane domain would be divided in such a way that it will be composed of an area that binds FAD and another region that binds inhibitors. The binding interactions of all the compounds within the active pocket is given in ESI (Table S5).†

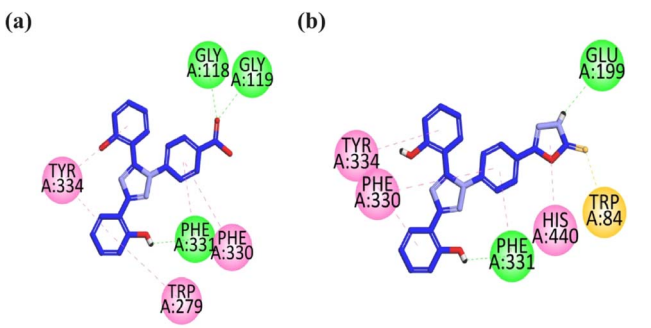


Fig. 2 2D interaction plot of compounds **9** (a) and **13** (b) in the binding site of AChE (1EVE), modeled using the Discovery Studio Visualizer.

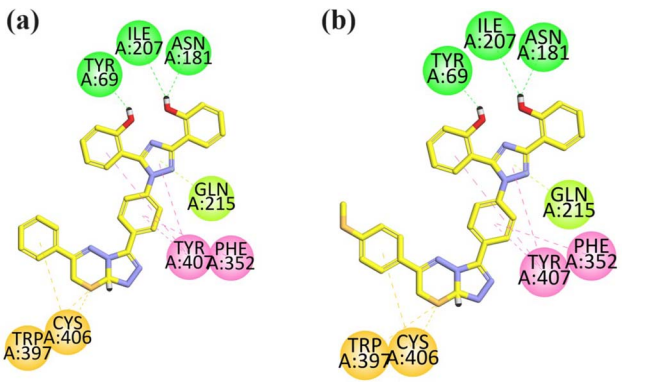


Fig. 4 2D interaction plot of compounds **18** (a) and **21** (b) in the binding site of MAO-A (2Z5X), modeled using Discovery Studio Visualizer.

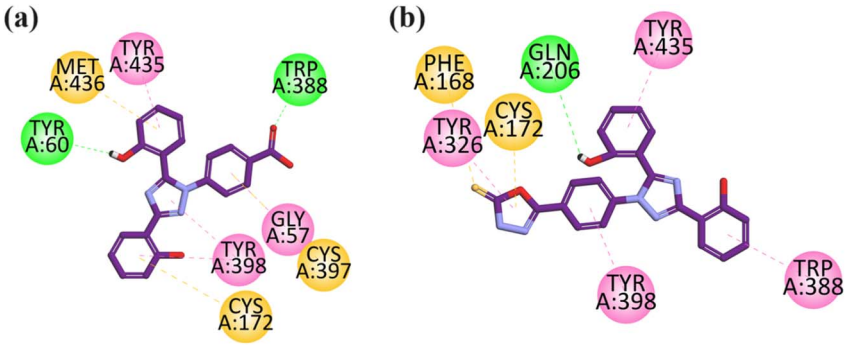


Fig. 5 2D interaction plot of compounds **9** (a) and **12** (b) in the binding site of MAO-B (2V5Z), modeled using Discovery Studio Visualizer.

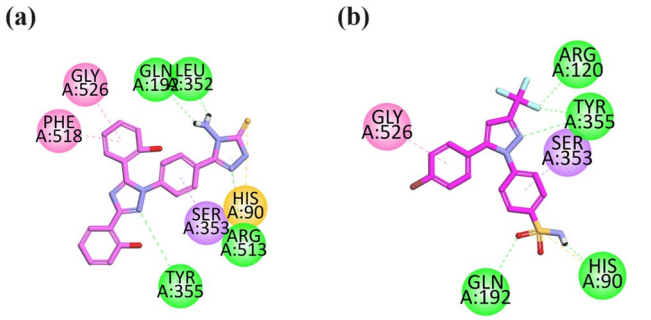


Fig. 6 2D interaction plot of compounds **13** (a) and celecoxib (b) in the binding site of COX-2 (1CX2), modeled using Discovery Studio Visualizer.

Visual inspection of compound **18** in the active site of MAO-A revealed that the compound exhibited three hydrogen bond interactions with TYR69, ASN181, and ILE207 due to two –OH groups attached to the aromatic ring. The aromatic rings formed hydrophobic interaction (pi–pi) with TYR40 and PHE352 amino acid residues. One of the pi–lone pair interactions was observed by the triazole ring with GLN215. Two pi–sulfur interactions were displayed by the sulfur atom present in the ring with Cys406 and Trp397 (Fig. 4a).

The compound **21** was analyzed for its interactions within the active site of MAO-A. Structural analysis revealed that the compound showed three key hydrogen bond interactions involving TYR69, ASN181, ILE207, facilitated by two hydroxyl groups (–OH) attached to its aromatic ring, which helped in the stability of the complex. Additionally, the aromatic rings of the compound participated in hydrophobic (pi–pi) interactions with TYR40 and PHE352. The triazole ring of the compound formed a π–lone pair interaction with GLN215. Furthermore, the sulfur atom within the ring structure engaged in two π–sulfur interactions with CYS406 and TRP397 (Fig. 4b).

**2.4.4 Binding mode of compound 9 and compound 12 in the binding site of MAO-B.** Similar to MAO-A, MAO-B is made up of two distinct domains, a membrane binding domain and an auxiliary membrane. The additional membrane binding domain is made up of two different regions, the FAD and inhibitor/substrate binding area. The binding interactions of all the compounds within the active pocket are given in the ESI (Table S5).†

Visual inspection of the binding mode of compound **9** in the binding site of MAO-B revealed that one hydrogen bond interaction is formed between the carbonyl group and TRP388, and another hydrogen bond interaction is formed by the hydroxyl group of the aromatic ring with TYR60 toward the C-terminal (substrate binding site). The aromatic rings display pi–sulfur interactions with MET436, CYS397, and CYS172 (substrate binding site). TYR435 and TYR398 exhibit hydrogen bond interaction with the aromatic region in the substrate binding site, and also show hydrophobic interaction (pi–pi) with the aromatic ring of GLY57. The important interactions displayed by this compound are with the TYR435, TYR398, CYS172, and TYR60 amino acid residues (substrate binding region) (Fig. 5a).

Visual inspection of compound **12** in the binding site of MAO-B revealed that TYR435, TYR398, TYR326, and TRP588 lie

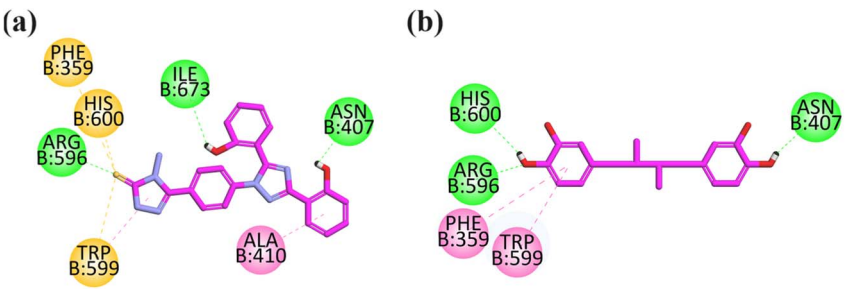


Fig. 7 2D interaction plot of compounds **13** (a) and nordihydroguaiaretic acid (b) in the binding site of 5-LOX (6N2W), modeled using the Discovery Studio Visualizer.

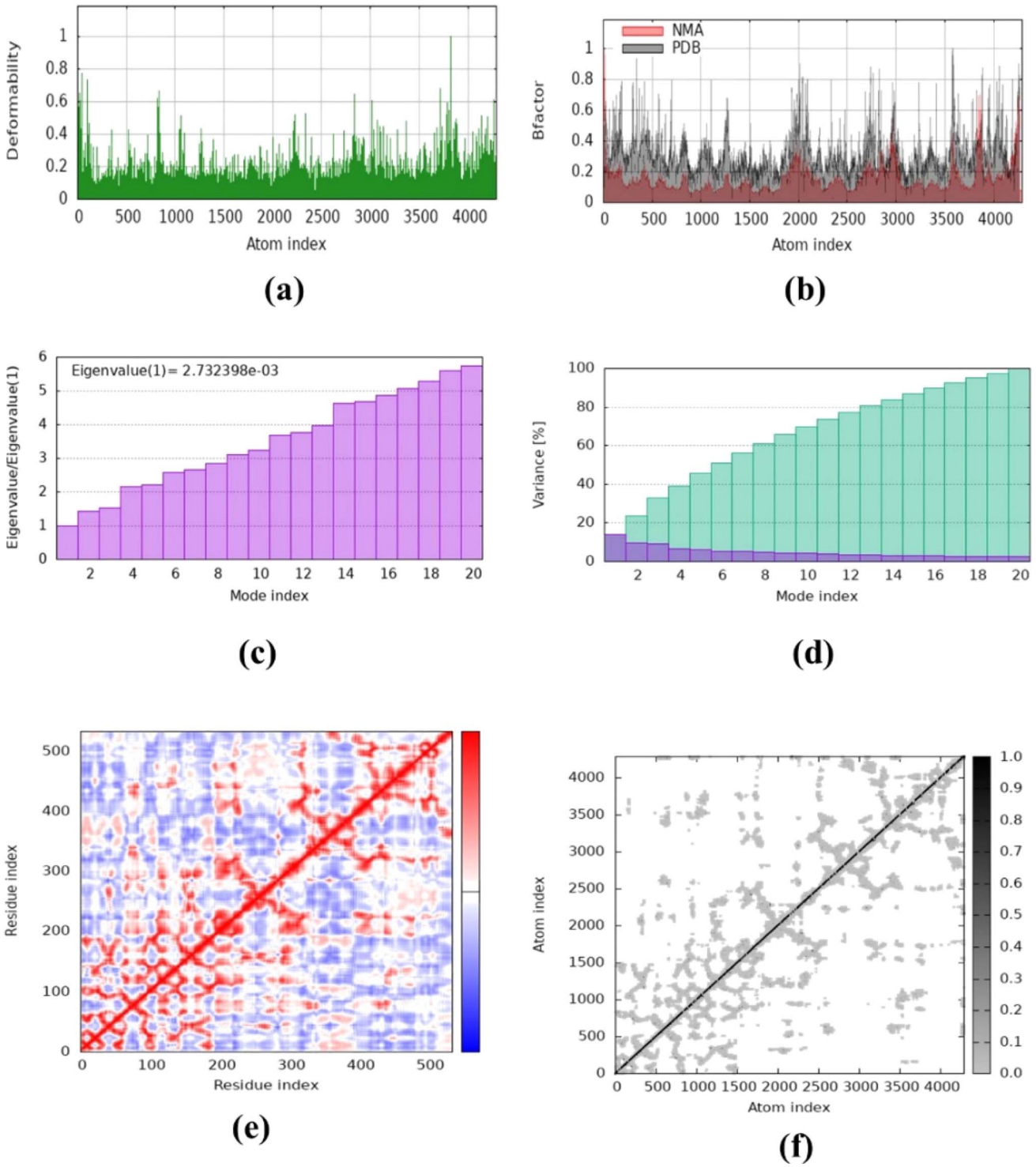


Fig. 8 Molecular dynamics simulation of complex **11** (AChE) using iMODS. (a) Deformability, (b) *B*-factor values, (c) eigenvalue, (d) variance, (e) co-variance and (f) elastic network model.

in the aromatic region and exhibit hydrophobic interaction (pi–pi) towards the C-terminal (substrate binding site). The –OH group of the aromatic rings display hydrogen bond interaction with Gln 206 toward the entrance cavity (Fig. 5b).

**2.4.5 Binding mode of compound 13 in the active site of COX-2 and standard drug.** According to the molecular modeling studies, compound **13**, which had powerful inhibitory action, was docked into the active site of COX-2 (PBD ID = 1CX2). This PBD COX-2 has S58 as a selective inhibitor. Initially the docking of S58 was done to determine the binding affinities. The selective inhibitor of COX-2, which is a native ligand, exhibits binding affinities with significant residues. These include

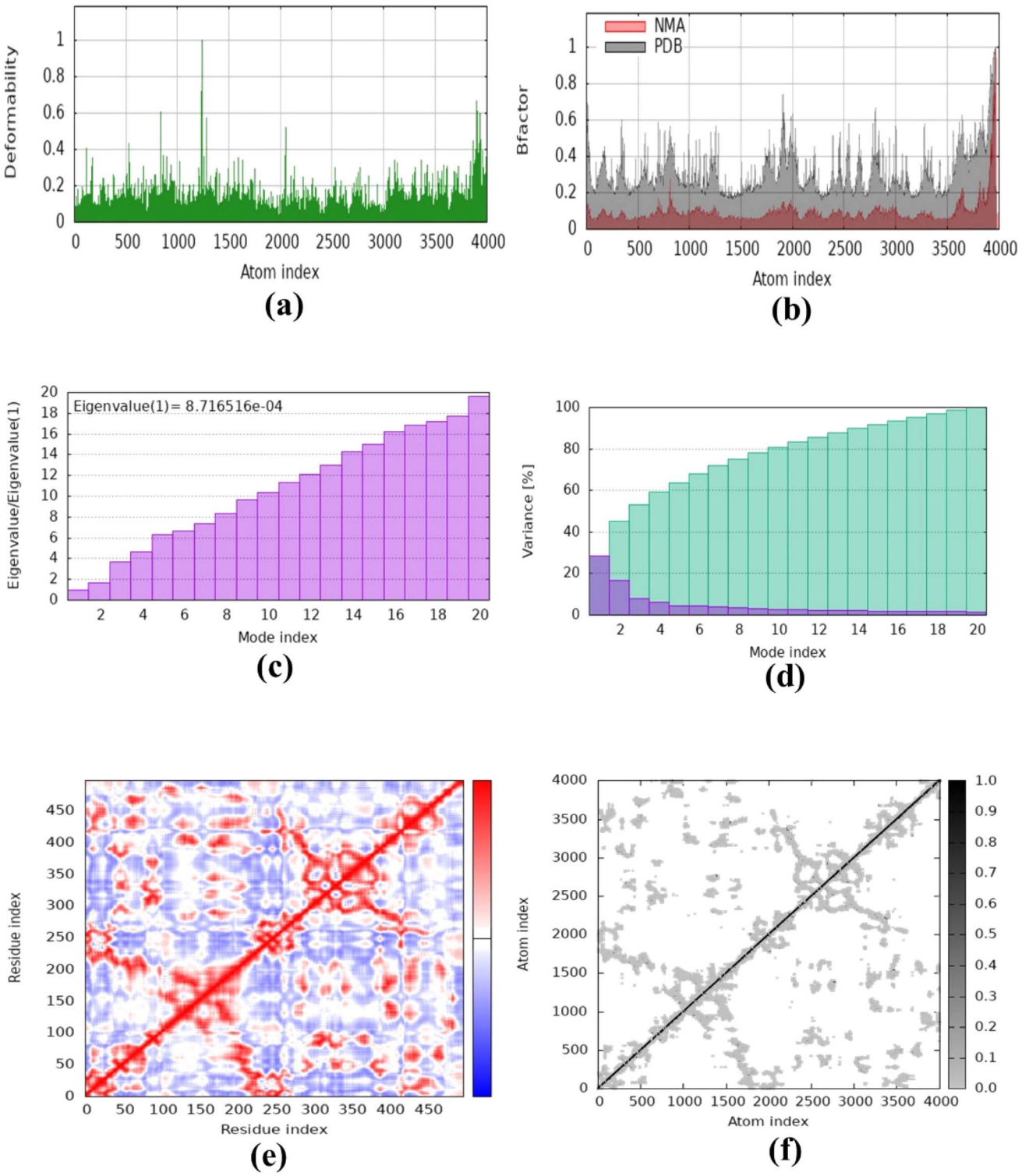


Fig. 9 Molecular dynamics simulation of complex **11** (MAO-B) using iMODS. (a) Deformability, (b) *B*-factor values, (c) eigenvalue, (d) variance, (e) co-variance and (f) elastic network model.

hydrophilic binding affinities with the COX-2 pocket residue (ARG513, ASP515, LEU352, SER353, and HIS90), hydrophobic interactions with VAL349, VAL523, TYR385, and TRP387, and hydrophilic binding affinities with TYR355, ARG120. The binding interactions of all the compounds within the active pocket are given in the ESI (Table S6).†

The visual inspection of the binding mode of compound **13** in the binding site of COX-2 revealed that 4-amino-2,4-dihydro-

3*H*-1,2,4-triazole-3-thione has strong binding interactions within the selective pocket region. It forms pi–sulfur interaction with HIS90, hydrophilic interaction with ARG513, and hydrophobic interaction with GLN192 and LEU352. The aromatic ring attached to triazole displays pi–sigma interaction in the selective pocket region with SER353. The triazole ring displays hydrophilic interaction with TYR355. The hydroxyl group containing an aromatic ring displays pi–pi interaction with PHE518. This compound orients toward the selective pocket region of COX-2 *via* HIS90, ARG513, SER353 and PHE518 (Fig. 6a).

The co-crystalized selective inhibitor (native ligand) of COX-2 forms binding affinities with important residues including hydrophilic binding affinities with the COX-2 residue (ARG120,

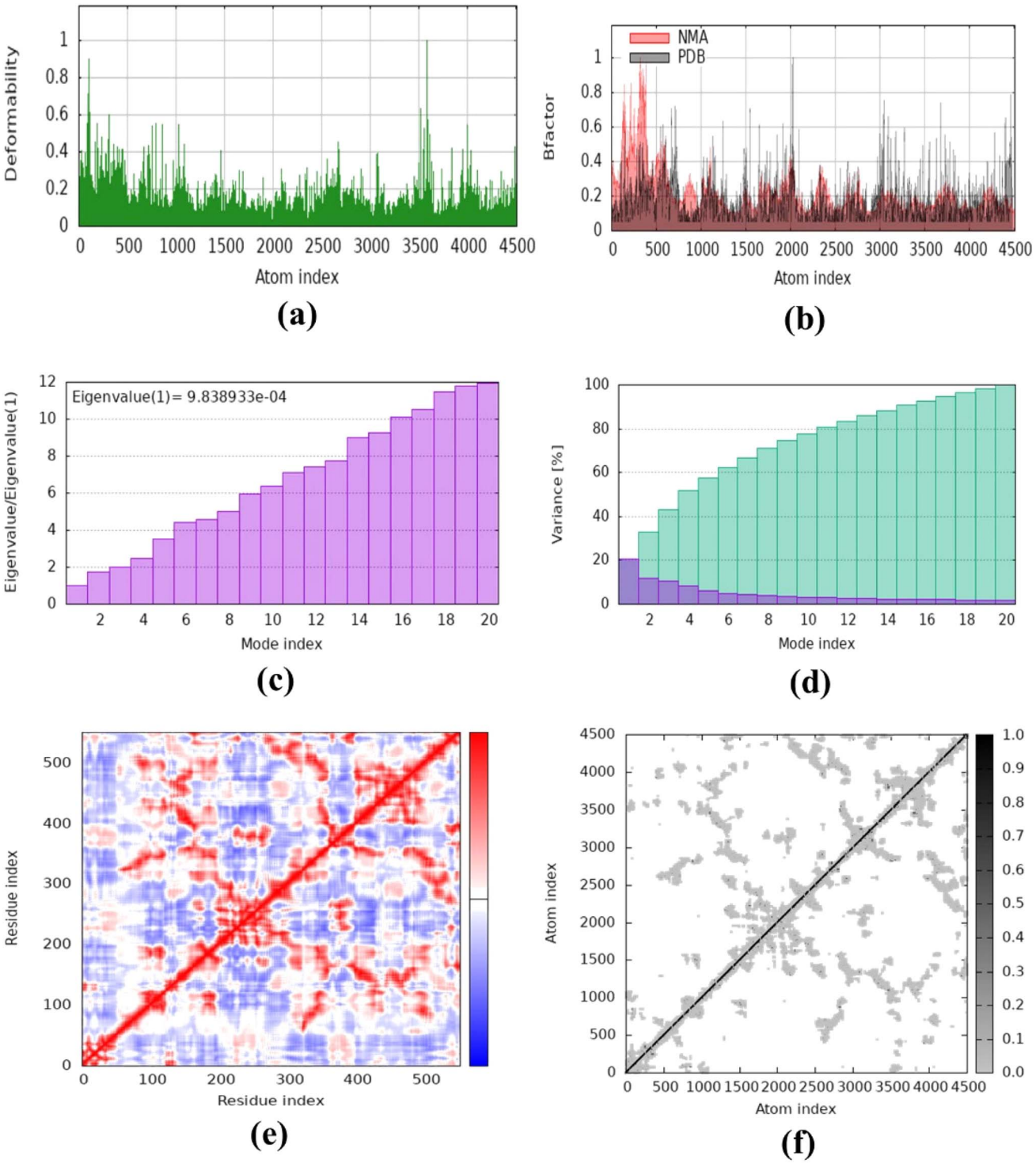


Fig. 10 Molecular dynamics simulation of complex **13** (COX-2) using iMODS. (a) Deformability, (b) *B*-factor values, (c) eigenvalue, (d) variance, (e) co-variance and (f) elastic network model.

TYR355, GLN192, and HIS90), hydrophobic interactions with GLY526 and pi–sigma interaction with SER353 (Fig. 6b).

**2.4.6 Binding mode of 13 in the active site of 5-LOX and standard drug.** To determine the binding affinities and interaction with amino acid residues, compound **13** was docked in the binding site of 5-lipoxygenase (5-LOX) (Table S6†). In the docking study, the co-crystallized structure of 5-lipoxygenase (6N2W) with nordihydroguaiaretic acid (NDGA) was used. Important residues such as HIS600, ASN407, LEU607, TRP599, ARG596, PHE359, HIS372, and ALA410 were shown to have binding affinities with NDGA.

Visual inspection revealed that compound **13** orients itself in the pocket of 5-LOX with two –OH groups attached to the aromatic ring forming H-bonds (hydrophilic binding affinity) with important residues including ILE673 and ASN407, which is an important interaction explaining the stability of the drug–ligand complex. The hydrophobic interaction (pi–pi) with ALA410 is displayed by an aromatic ring attached with a hydroxyl ring at one end and a triazole ring at another end. The carbonyl group of 4-amino-2,4-dihydro-3*H*-1,2,4-triazole-3-thione displays three pi–sulfur interactions with PHE359 and HIS600 (Fig. 7a).

The co-crystallized structure of 5-lipoxygenase (6N2W) with nordihydroguaiaretic acid (NDGA) was selected for the docking analysis. NDGA showed hydrogen binding affinities with important residues including HIS600, ARG596, and ASN407, and hydrophobic interaction with PHE359 and TRP599 (Fig. 7b).

According to the molecular docking results, the results were found to be consistent with the *in vitro* investigations, suggesting that compound **11** is the most potent compound as a multi-targeting agent.

### 2.5 Molecular dynamics simulation

The molecular dynamics simulation was carried out to evaluate the strength, movement of atoms, and stiffness of the highest ranked docked pose of protein complexes **11** (AChE and MAO-B) and **13** (COX2). This was accomplished by utilizing the online web server iMOD (**https://imods.iqf.csic.es/**, which was accessed on August 23, 2024) and the outcomes of the docked complexes are shown in Fig. 7. The graphs describing the deformability of the protein complexes are shown in Fig. 8. The placement of various hinges, both high and low, illustrates the area of residues that are distorted in the docked complexes. Through the use of the experimental *B*-factor, the value of root mean square (RMS) was established, hence revealing the unpredictability of atoms inside the protein complexes. According to the supplied data, the eigenvalues of compounds **11** and **13** were found to be $2.732398 \times 10{-}^{33}$, $8.716516 \times 10{-}^{44}$, and $9.838933 \times 10{-}^{44}$ for AChE, MAO-B, and COX-2, respectively. The eigenvalue is linked to the normal mode and demonstrates motion inflexibility, and it is proportional to the binding energy that is associated with the process of deforming the globular structure of the protein. The variance graph of amino acid residues is shown in Fig. 9, illustrating how the eigenvalue is inversely proportional to the variance. Alternatively, the covariance matrix, as shown in Fig. 7–9, stipulates that the pairing between amino acid residues experiences movements in distinct colors. These colors include red (correlated), white (uncorrelated), and blue (anti-correlated). The coupling pair of atoms that are considered to be related with springs is characterized by the elastic model. As can be seen in Fig. 8–10, the various dots, which are grey in color, that are present in the graph represent one spring between the interrelating atoms that constitute the inelastic springs.

### 2.6. ADMET analysis

The investigation focused on assessing the physicochemical characteristics of the synthesized hybrid compounds **9–11**, **13**, **15** and **16–25** utilizing the SwissADME tool.[34] The detailed description is provided in the ESI File.†

## 3 Conclusions

This study described the synthesis and evaluation of new compounds aimed at addressing Alzheimer's disease (AD), a major cause of dementia worldwide. Given the complex nature of AD, characterized by both neuroinflammation and disruptions in lipid metabolism, there is a significant need for drugs that can target multiple pathways simultaneously. This study involved the synthesis of triazolo-thiadiazine derivatives of deferasirox, aiming to create multi-target compounds that can inhibit the above-mentioned enzymes. In particular, compound **11** shows potential as a lead molecule due to its strong inhibitory effects on AChE, MAO-B, and COX-2. Other compounds, such as **9** and **13**, also showed dual inhibition, with their performance surpassing that of the standard drugs. The simulations and physicochemical properties of the lead compounds support their potential as promising candidates for treating multifactorial diseases such as AD, which involve neuroinflammation. Conclusively, this research paves the way for the further development of these hybrid compounds as potential treatments for AD, aiming to provide more effective disease-modifying therapies.

## 4 Experimental

### 4.1. Materials and methods

All chemicals and reagents: deferasirox, hydrazine monohydrate, carbon disulfide ($CS_2$), potassium hydroxide (KOH), substituted acetophenones, acetic acid, sulphuric acid ($H_2SO_4$), *n*-hexane, ethyl acetate, diethyl ether, acetone, methanol and ethanol were purchased from Sigma Aldrich.

**4.1.1 General method for the synthesis of deferasirox-substituted ester (10).** The synthesis of deferasirox-substituted ester (**10**) was carried out by dissolving deferasirox in excess methanol in the presence of $H_2SO_4$ and refluxing for 8 h. Completion of the reaction was confirmed by TLC, after which the reaction mixture was concentrated on a rotary evaporator and purified by solvent extraction.

Transparent oily liquid. Yield: 55%, Rf = 0.7, (*n*-hexane/ethyl acetate = 2 : 3), M.P: 194–196 °C, FT-IR (KBr disc) γmax ($cm^{-1}$):

3280 (O–H), 2920 (C–H), 1721 (C=O), 1587 (C=C), 1491 (C=N), 1465 (C–N), 1277 (C–O). $^1$H NMR (400 MHz, DMSO-$d_6$) δ 10.78 (s, 1H, OH), 8.15–8.10 (m, 2H), 8.03 (dd, $J$ = 13.0, 7.9 Hz, 4H), 7.57 (dd, $J$ = 12.6, 7.8 Hz, 3H), 7.38 (q, $J$ = 7.5 Hz, 3H), 7.00 (m, 5H), 6.86 (d, $J$ = 8.2 Hz, 1H), 3.86 (s, 3H).[21]

**4.1.2 General method for the synthesis of deferasirox-substituted hydrazide (11).** Deferasirox-substituted hydrazide was synthesized by reacting the ester of deferasirox with hydrazine in the presence of ethanol. After the completion of the reaction, the mixture was concentrated on a rotary evaporator and washed with chilled methanol to obtain deferasirox-substituted hydrazide (**11**).[21]

White solid. Yield: 90%, Rf = 0.4, (*n*-hexane/ethyl acetate = 3 : 2), M.P: 259–261 °C, FT-IR (KBr disc) γmax (cm$^{-1}$): 3297 (O–H),3185 (N–H), 3058 (C–H), 1702 (C=O), 1608 (C=C), 1492 (C=N), 1460 (C–N), 1289 (C–O). $^1$H NMR (400 MHz, DMSO-$d_6$) δ: 10.83 (s, 1H, OH-24), 10.08 (s, 1H, NH-28), 9.87 (s, 1H, OH-25), 8.04 (d, 1H, Ar-H-9), 7.87 (d, $J$ = 8.3 Hz, 2H, Ar-H-20 & Ar-H-22), 7.56–7.48 (m, 3H, Ar-H-18, Ar- 34 H-19 & Ar-H-23), 7.42–7.33 (m, 2H, Ar-H-11 & Ar-H-16), 7.06–6.94 (m, 3H, Ar-H-10, ArH-12 & Ar-H-17), 6.86 (d, $J$ = 8.2 Hz, 1H, Ar-H-15), 4.55 (s, 2H, NH2-29), $^{13}$C NMR (150 MHz, DMSO-$d_6$) δ 165.1, 160.2, 156.8, 155.7, 152.4, 140.2, 132.9, 132.5, 131.8, 131.5, 129.0, 128.4, 127.2, 123.8, 123.7, 120.1, 119.8, 117.5, 116.6, 114.9, 114.1.

**4.1.3 General method for the synthesis of deferasirox-substituted 1,3,4-oxadizole (12).** Deferasirox hydrazide was reacted with carbon disulphide ($CS_2$) in the presence of ethanol as the solvent followed by the addition of a few pellets of potassium hydroxide (KOH) as a catalyst. The mixture was refluxed for 10–12 h. The white precipitate of compound **12** was filtered washed with diethyl ether and subjected to next step for the synthesis of compound **13**.[21]

**4.1.4 General method for the synthesis of deferasirox-substituted 1,2,4-tirazolesamine (13).** Compound **12** was reacted with hydrazine monohydrate ($NH_2$–$NH_2 \cdot H_2O$) in ethanol as the solvent and the reaction mixture was refluxed for 72 h. On completion of the reaction, water was added to the mixture and the solution acidified with conc. HCl, causing the desired product (**13**) to precipitate. The as-obtained crude was purified by recrystallization using methanol.[21]

Light-yellowish solid, Yield: 70%, Rf = 0.6, (*n*-hexane/ethyl acetate = 2 : 3), M.P: 294–296 °C, FT-IR (KBr disc) γmax (cm$^{-1}$): 3308 (O–H), 3209 (N–H), 3075 (C–H), 1615 (C=C), 1584 (C=N), 1514 (C–N), 1294 (C–O),1155 (C=S), $^1$H NMR (400 MHz, DMSO-$d_6$) δ: 14.02 (s, 1H, NH-29), 10.82 (s, 1H, OH-24), 10.15 (s, 1H, OH-25), 8.10 (d, $J$ = 8.5 Hz, 2H, Ar-H-20 & Ar-H-22), 8.05 (dd, $J$ = 7.8, 1.7 Hz, 1H, Ar-H-9), 7.60 (d, 2H, Ar-H-19 & Ar-H-23), 7.56 (dd, $J$ = 7.7, 1.7 Hz, 1H, Ar-H-18), 7.43–7.33 (m, 2H, Ar-H-11 & Ar-H-16), 7.06–6.95 (m, 3H, Ar-H-10, Ar-H-12 & Ar-H-17), 6.88 (d, $J$ = 8.2 Hz, 1H, Ar-H-15), 5.80 (s, 2H, $NH_2$-30). $^{13}$C NMR (100 MHz, DMSO-$d_6$) δ: 167.7, 160.3, 156.8, 155.7, 152.4, 149.1, 139.7, 133.0, 131.9, 131.6, 129.3, 127.2, 126.1, 123.9, 120.2, 119.9, 117.5, 116.6, 114.9, 114.1.[21]

**4.1.5 General procedure for the synthesis of α-bromoacetophenone (14a–k).** For the synthesis of α-bromoacetophenone, substituted acetophenones were treated with bromine at 0 °C for one hour. The obtained precipitates were filtered and washed with ether (Scheme 2).

**4.1.6 General procedure for the synthesis of triazolothiadiazines.** Condensation of the triazole amine and α-bromoacetophenone was carried out in ethanol. The reaction mixture was refluxed for six to seven hours. Completion of the reaction was observed by TLC. Upon completion, the reaction mixture was concentrated on a rotary evaporator and the as-obtained solid was purified by column chromatography using solvent system: *n*-hexane:ethyl acetate (Scheme 3).

**4.1.7 2,2′-(1-(4-(6-(4-Chlorophenyl)-7*H*-[1,2,4]triazolo[3,4-*b*][1,3,4]thiadiazin-3-yl)phenyl)-1*H*-1,2,4-triazole-3,5-diyl) diphenol (15).** Off-white solid, Yield: 70%, Rf = 0.7, (*n*-hexane/ethyl acetate = 2 : 3), M.P: 250–252 °C, FT-IR (KBr disc) γmax (cm$^{-1}$): 3061 (O–H), 2850 (C–H), 1612 (C=C), 1587 (C=N), 1453 (C–N), 1249 (C–O), 848 (C–Cl), 760 (C–S–C), $^1$H NMR (400 MHz, DMSO-$d_6$) δ 10.84 (s, 1H), 10.12 (s, 1H), 8.16 (d, $J$ = 8.2 Hz, 2H), 8.12–8.02 (m, 5H), 7.65 (d, $J$ = 8.6 Hz, 2H), 7.57 (dd, $J$ = 7.7, 1.7 Hz, 1H), 7.45–7.33 (m, 2H), 7.06–6.95 (m, 3H), 6.88 (d, $J$ = 8.2 Hz, 1H), 4.47 (s, 2H); $^{13}$C NMR (100 MHz, DMSO-$d_6$) δ 159.8, 156.3, 155.2, 154.9, 151.9, 150.9, 142.8, 139.1, 137.6, 133.0, 132.5, 131.4, 131.1, 128.7, 128.4, 126.7, 125.6, 123.6, 119.7, 119.4, 118.2, 117.0, 116.1, 114.4, 114.0, 113.7, 56.0, 23.2, HRMS (ESI) $m/z$, Calcd. for ($C_{30}H_{20}ClN_7O_2S$ + $H^+$) 578.05, Found 569.2614.

**4.1.8 2,2′-(1-(4-(6-(3-Nitrophenyl)-1,8a-dihydro-7*H*-[1,2,4]triazolo[3,4-*b*][1,3,4]thiadiazin-3-yl)phenyl)-1*H*-1,2,4-triazole-3,5-diyl)diphenol (16).** Light yellow solid, Yield: 75%, Rf = 0.5, (*n*-hexane/ethyl acetate = 3 : 2), M.P: 233–235 °C, FT-IR (KBr disc) γmax (cm$^{-1}$): 3252 (O–H), 3088 (C–H), 1621 (C=C), 1587 (C=N), 1530 (O=N=O), 1494 (C–N), 1253 (C–O), 760 (C–S–C); $^1$H NMR (400 MHz, DMSO-$d_6$) δ 10.84 (s, 1H), 10.13 (s, 1H), 8.76 (t, $J$ = 2.0 Hz, 1H), 8.43 (ddd, $J$ = 13.1, 7.8, 2.0 Hz, 2H), 8.12–8.00 (m, 3H), 7.87 (t, $J$ = 8.0, 1.3 Hz, 1H), 7.69–7.61 (m, 2H), 7.57 (dd, $J$ = 7.7, 1.7 Hz, 1H), 7.38 (m, 2H), 7.06–6.94 (m, 3H), 6.88 (d, $J$ = 8.2 Hz, 1H), 4.52 (s, 2H); $^{13}$C NMR (100 MHz, DMSO-$d_6$) δ 160.3, 156.8, 155.7, 155.0, 152.4, 151.3, 148.7, 143.4, 139.5, 135.5, 134.1, 132.9, 131.9, 131.5, 131.2, 129.2, 127.2, 126.8, 126.0, 124.0, 122.8, 120.1, 119.9, 117.5, 116.5, 114.9, 114.1, 23.4, HRMS (ESI) $m/z$, Calcd. for ($C_{30}H_{20}N_8O_4S$ + $H^+$) 588.6, Found 589.6000.

**4.1.9 4-(3-(4-(3,5-Bis(2-hydroxyphenyl)-1*H*-1,2,4-triazol-1-yl) phenyl)-1,8*a*-dihydro-7*H*-[1,2,4]triazolo[3,4-*b*][1,3,4]thiadiazin-6-yl)benzonitrile (17).** Brown solid, Yield: 80%, Rf = 0.6, (*n*-hexane/ethyl acetate = 3 : 2), M.P: 280–282 °C. FT-IR (KBr disc) γmax (cm$^{-1}$): 3319 (O–H), 3059 (C–H), 2226 (C≡N), 1612 (C=C), 1587 (C=N), 1455 (C–N), 1299 (C–O), 759 (C–S–C)$^1$H NMR (400 MHz, DMSO-$d_6$) δ 10.84 (s, 1H), 10.12 (s, 1H), 8.16 (d, $J$ = 8.2 Hz, 2H), 8.06 (dd, $J$ = 8.5, 3.1 Hz, 5H), 7.65 (d, $J$ = 8.4 Hz, 2H), 7.57 (dd, $J$ = 7.6, 1.7 Hz, 1H), 7.45–7.33 (m, 2H), 7.06–6.95 (m, 3H), 6.88 (d, $J$ = 8.2 Hz, 1H), 4.47 (s, 2H); $^{13}$C NMR (100 MHz, DMSO-$d_6$) δ 160.3, 156.8, 155.7, 155.3, 152.4, 151.3, 143.3, 139.5, 138.0, 133.4, 133.0, 131.9, 131.5, 129.2, 128.8, 127.2, 126.0, 124.1, 120.1, 119.9, 118.7, 117.5, 116.5, 114.9, 114.5, 114.1, 23.2 HRMS (ESI) $m/z$, Calcd. for ($C_{31}H_{20}N_8O_2S$ + $H^+$) 568.6, Found 569.6130.

**4.1.10 2,2′-(1-(4-(6-phenyl-1,8a-dihydro-7H-[1,2,4]triazolo[3,4-*b*][1,3,4]thiadiazin-3-yl)phenyl)-1*H*-1,2,4-triazole-3,5-diyl)**

**diphenol (18).** White solid, Yield: 60%, Rf = 0.7, (*n*-hexane/ethyl acetate = 2 : 3), M.P: 282–284 °C. FT-IR (KBr disc) γmax ($cm^{-1}$): 3632 (O–H), 3058 (C–H), 1613 (C=C), 1582 (C=N), 1457 (C–N), 1299 (C–O), 757 (C–S–C) $^1$H NMR (400 MHz, DMSO-$d_6$) δ 10.84 (s, 1H), 10.11 (s, 1H), 8.12–7.97 (m, 5H), 7.69–7.53 (m, 6H), 7.45–7.33 (m, 2H), 7.07–6.95 (m, 3H), 6.89 (d, $J$ = 8.3 Hz, 1H), 4.45 (s, 2H); $^{13}$C NMR (100 MHz, DMSO-$d_6$) δ 160.3, 156.8, 156.7, 155.7, 152.4, 151.2, 143.4, 139.4, 133.8, 132.96, 132.5, 131.9, 131.5, 129.6, 129.1, 128.1, 127.2, 126.2, 124.1, 120.1, 119.9, 117.5, 116.5, 114.9, 114.1, 23.2; HRMS (ESI) *m*/*z*, Calcd. for ($C_{30}H_{21}N_7O_2S$ + $H^+$) 543.63, Found 544.6383.

**4.1.11 2,2′-(1-(4-(6-(4-Methoxyphenyl)-1,8*a*-dihydro-7*H*-[1,2,4]triazolo[3,4-*b*][1,3,4]thiadiazin-3-yl)phenyl)-1*H*-1,2,4-triazole-3,5-diyl)diphenol (19).** Brownish solid, Yield: 65%, Rf = 0.6, (*n*-hexane/ethyl acetate = 4 : 1), M.P: 258–260 °C. FT-IR (KBr disc) γmax ($cm^{-1}$): 3193 (O–H), 3055 (C–H), 1588 (C=C), 1513 (C=N), 1459 (C–N), 1299 (C–O), 753 (C–S–C).$^1$H NMR (400 MHz, DMSO-$d_6$) δ 10.84 (s, 1H), 10.12 (s, 1H), 8.08 (dd, $J$ = 11.0, 8.3 Hz, 3H), 8.02–7.95 (m, 2H), 7.64 (d, $J$ = 8.5 Hz, 1H), 7.57 (dd, $J$ = 7.6, 1.7 Hz, 2H), 7.39 (d, $J$ = 8.3 Hz, 2H), 7.12 (d, $J$ = 8.7 Hz, 1H), 7.07–6.93 (m, 4H), 6.88 (d, $J$ = 8.3 Hz, 1H), 4.40 (s, 1H), 3.86 (s, 4H); $^{13}$C NMR (100 MHz, DMSO-$d_6$, DEPT-135) δ: 132.9, 131.9, 131.5, 130.2, 129.0, 127.2, 124.0, 120.1, 117.5, 116.5, 115.0, 23.4, HRMS (ESI) *m*/*z*, Calcd. for ($C_{31}H_{23}N_7O_3S$ + $H^+$) 573.63, Found 574.6562.

**4.1.12 2,2′-(1-(4-(6-(2-Hydroxyphenyl)-1,8*a*-dihydro-7H-[1,2,4]triazolo[3,4-*b*][1,3,4]thiadiazin-3-yl)phenyl)-1*H*-1,2,4-triazole-3,5-diyl)diphenol (20).** Yellowish solid. Yield: 56%, Rf = 0.8, (*n*-Hexane/Ethyl acetate = 2 : 3), M.P: 273–275 °C. FT-IR (KBr disc) γmax ($cm^{-1}$): 3260 (O–H), 3047 (C–H), 1622 (C=C), 1588 (C=N), 1462 (C–N), 1285 (C–O), 751 (C–S–C). $^1$H NMR (400 MHz, DMSO-$d_6$) δ 10.93 (s, 1H), 10.81 (s, 1H), 10.10 (s, 1H), 8.09–8.01 (m, 3H), 7.67–7.62 (m, 2H), 7.65–7.50 (m, 3H), 7.42–7.32 (m, 2H), 6.99 (ddd, $J$ = 16.7, 7.9, 3.5 Hz, 5H), 6.87 (d, $J$ = 8.2 Hz, 1H), 4.28 (s, 2H); $^{13}$C NMR (100 MHz, DMSO-$d_6$, DEPT-135) δ:135.6, 132.9, 132.3, 131.8, 131.5, 129.0, 127.2, 124.0, 120.1, 119.8, 119.2, 117.5, 116.5, 23.4.

**4.1.13 2,2′-(1-(4-(6-(4-(Methylthio)phenyl)-1,8*a*-dihydro-7*H*-[1,2,4]triazolo[3,4-b][1,3,4]thiadiazin-3-yl)phenyl)-1*H*-1,2,4-triazole-3,5-diyl)diphenol (21).** Brownish solid, Yield: 52%, Rf = 0.7, (*n*-hexane/ethyl acetate = 2 : 3), M.P: 230–232 °C. FT-IR (KBr disc) γmax ($cm^{-1}$): 3066 (O–H), 2981 (C–H), 1620 (C=C), 1583 (C=N), 1460 (C–N), 1353 (C–O), 750 (C–S–C). $^1$H NMR (400 MHz, DMSO-$d_6$) δ 10.80 (s, 1H), 10.14 (s, 1H), 8.11–8.04 (m, 3H), 7.86 (d, $J$ = 8.4, 1H), 7.60–7.56 (m, 3H), 7.41–7.31 (m, 4H), 7.02–6.95 (m, 4H), 6.87 (d, $J$ = 8.4, 1H), 5.80 (s, 2H), 1.39 (s, 3H, $SCH_3$), HRMS (ESI) *m*/*z*, Calcd. for ($C_{31}H_{23}N_7O_2S_2$ + $H^+$) 589.60, Found 590.6937.

**4.1.14 3-(3-(4-(3,5-Bis(2-hydroxyphenyl)-1*H*-1,2,4-triazol-1-yl)phenyl)-1,8*a*-dihydro-7*H*-[1,2,4]triazolo[3,4-*b*][1,3,4]thiadiazin-6-yl)-3,10*a*-dihydro-2*H*-benzo[*g*]chromen-2-one (22).** FT-IR (KBr disc) γmax ($cm^{-1}$): 3256 (O–H), 2928 (C–H), 1717 (C=O), 1620 (C=C), 1587 (C=N), 1461 (C–N), 1353 (C–O), 752 (C–S–C). $^1$H NMR (400 MHz, DMSO-$d_6$) δ 10.84 (s, 1H), 10.12 (s, 1H), 8.16 (d, $J$ = 8.2 Hz, 2H), 8.06 (m, 3H), 7.65 (d, $J$ = 8.4 Hz, 2H), 7.57 (dd, $J$ = 7.6, 1.7 Hz, 1H), 7.45–7.33 (m, 2H), 7.30–7.10 (m, 3H), 7.06–6.95 (m, 3H), 6.88 (d, $J$ = 8.2 Hz, 1H), 4.47 (s, 2H).

**4.1.15 3-(3-(4-(3,5-Bis(2-hydroxyphenyl)-1*H*-1,2,4-triazol-1-yl)phenyl)-1,8*a*-dihydro-7*H*-[1,2,4]triazolo[3,4-*b*][1,3,4]thiadiazin-6-yl)-7-bromo-3,8*a*-dihydro-2*H*-chromen-2-one (23).** FT-IR (KBr disc) γmax ($cm^{-1}$): 3256 (O–H), 2928 (C–H), 1717 (C=O), 1620 (C=C), 1587 (C=N), 1461 (C–N), 1353 (C–O), 828 (C–Br), 752 (C–S–C). $^1$H NMR (400 MHz, DMSO-$d_6$) δ 10.84 (s, 1H), 10.13 (s, 1H), 8.76 (t, $J$ = 2.0 Hz, 1H), 8.43 (m, 2H), 8.12–8.00 (m, 3H), 7.87 (t, $J$ = 8.0 Hz, 1H), 7.69–7.61 (m, 2H), 7.57 (dd, $J$ = 7.7, 1.7 Hz, 1H), 7.38 (m, 2H), 7.06–6.94 (m, 3H), 6.88 (d, $J$ = 8.2 Hz, 1H), 4.52 (s, 2H).

**4.1.16 2,2′-(1-(4-(6-(4-Hydroxyphenyl)-1,8*a*-dihydro-7*H*-[1,2,4]triazolo[3,4-*b*][1,3,4]thiadiazin-3-yl)phenyl)-1*H*-1,2,4-triazole-3,5-diyl)diphenol (24).** FT-IR (KBr disc) γmax ($cm^{-1}$): 3056 (O–H), 2950 (C–H), 1587 (C=C), 1514 (C=N), 1457 (C–N), 1228 (C–O), 752 (C–S–C). $^1$H NMR (400 MHz, DMSO-$d_6$) δ 10.84 (s, 1H), 10.12 (s, 1H), 8.16 (d, $J$ = 8.2 Hz, 2H), 8.12–8.02 (m, 4H), 7.65 (d, $J$ = 8.6 Hz, 2H), 7.57 (dd, $J$ = 7.7, 1.7 Hz, 1H), 7.45–7.33 (m, 2H), 7.06–6.95 (m, 3H), 6.72 (s, 1H), 6.88 (d, $J$ = 8.2 Hz, 1H), 4.47 (s, 2H). $^{13}$C NMR (101 MHz, DMSO-$d_6$) δ 161.8, 160.2, 156.8, 156.3, 155.8, 152.4, 150.9, 143.3, 139.3, 132.9, 131.9, 131.5, 130.1, 129.0, 127.2, 126.4, 124.0, 120.1, 119.8, 117.5, 116.5, 116.4, 114.9, 114.1, 22.9.

**4.1.17 2,2′-(1-(4-(6-(2,4-Dichlorophenyl)-1,8*a*-dihydro-7*H*-[1,2,4]triazolo[3,4-*b*][1,3,4]thiadiazin-3-yl)phenyl)-1*H*-1,2,4-triazole-3,5-diyl)diphenol (25).** FT-IR (KBr disc) γmax ($cm^{-1}$): 3061 (O–H), 2980 (C–H), 1693 (C=C), 1580 (C=N), 1491 (C–N), 1242 (C–O), 982 (C–Cl), 751 (C–S–C), $^1$H NMR (400 MHz, DMSO-$d_6$) δ: 10.81 (s, 1H), 10.09 (s, 1H), 8.05 (d, 1H, $J$ = 8.6), 7.91 (d, 1H, $J$ = 8.3), 7.88–7.85 (m, 3H), 7.79–7.74 (m, 4H), 7.37 (m, 3H), 6.08–6.87 (m, 3H), 4.32 (s, 2H), $^{13}$C NMR (101 MHz, DMSO-$d_6$) δ 160.2, 156.8, 156.5, 155.6, 152.3, 139.6, 136.8, 133.5, 133.2, 132.9, 131.9, 131.5, 131.1, 131.1, 130.9, 130.6, 130.3, 129.1, 128.0, 127.9, 127.2, 124.1, 120.1, 119.9, 117.5, 116.6, 114.8, 114.1, 67.9,23.4, HRMS (ESI) *m*/*z*, Calcd. for ($C_{30}H_{19}Cl_2N_7O_2S$) 612.49, Found 612.4974.

### 4.2. Biological assay

**4.2.1 Methodology for AChE and BChE.** The inhibition activities of the deferasirox derivatives (**10–13** and **15–25**) were carried out against AChE (EC Number: 3.1.1.7.) and BChE (EC 3.1.1.8) using a slightly modified Ellman's method.[35] For the preparation of 1 mM concentrated solution of samples for the assay, DMSO (10%) was used as the solvent. For each assay, 50 mM phosphate buffer at pH 7.8, 10 μL of compound under study (1 mM) and 10 μL of enzyme (0.029 and 0.5 U $mL^{-1}$ of AChE or BChE, respectively) were mixed and pre-incubated at 37 °C for 10 min. After the addition of 10 μL of 1 mM acetylthiocholine iodide or butyrylthiocholine chloride and 10 μL of 5,5-dithiobis-2-nitro benzoic acid reagent (5 mM), the enzymatic reactions were started. After 30 min, the progress of the enzymatic reaction was monitored spectrophotometrically at a wavelength of 405 nm using a Microplate reader (FLUOstar omega, BMG Labtech, Germany). Donepezil (1 mM) was used as the standard. The compounds with more than 50% inhibition in three replicates

were further diluted into eight different concentrations to calculate the $IC_{50}$ values by GraphPad Prism 8.4.3.[36]

**4.2.2 Methodology for MAO-A and MAO-B.** All the synthesised derivatives (**10–13** and **15–25**) were tested for their monoamine oxidase inhibition activity against MAO-A and MAO-B using the reported method.[34] The preparation of the enzyme was carried out for 15–20 min under cool environmental conditions. To irreversibly block the MAO-A and MAO-B activity clorgyline 60 nM or deprenyl 300 nM were used. 100 μL volume of the assay consisted of buffer (60 μL with pH 7.4), 10 μL test compound (0.1 mM, dissolved in DMSO 10%), followed by 10 μL of enzyme (26 μg of protein for MAO-A and 5.0 μg for MAO-B). After 15–20 min incubation with MAO-B and MAO-A was carried out, 10 μL and 10 μL freshly prepared Amplex Red were added to the mixture. The final concentration of clorgyline and deprenyl used to estimate the non-MAO A and MAO B activity was 0.1 mM, respectively. Using a fluorescence plate reader (BMG Labtech GmbH, Ortenberg, Germany), the change in the fluorescence was determined. The assay was replicated thrice. The $IC_{50}$ values of the compounds with more than 50% inhibition were calculated using non-linear curve fitting program PRISM 5.0 (GraphPad, San Diego, California, USA.[36]

**4.2.3 Methodology for COX-2 inhibition assay.** Cyclooxygenase (COX-2) from human recombinant (CAT No. C0858) and enzyme substrates arachidonic acid (CAT No. 150384) and linoleic acid (CAS No. 60-33-3) were all obtained from SIGMA ALDRICH. The indicator and co-factor compounds, including glutathione (CAS 70-18-8), *N*,*N*,*N*-tetramethyl-*p*-phenylenediamine dihydrochloride (TMPD) (CAS 637-01-4), and hematin (CAS 15489-90-4), were acquired from SIGMA ALDRICH.

COX-2 inhibition experiments were conducted using the Glassman and White methodology with minor modifications. The COX-2 enzyme (300 units per mL) was activated on ice for 5 min prior to the assay, followed by the introduction of a co-factor solution (50 μL) comprised of *N*,*N*,*N*,*N*-tetramethyl-*p*-phenylenediamine dihydrochloride (TMPD) (0.24 mM), glutathione (0.9 mM), and hematin (0.1 mM) in 0.1 M Tris HCl buffer at pH 8.0. Solutions of tested substances (20 μL) with varying concentrations from 31.25 to 1000 μg $mL^{-1}$ and enzyme solutions (60 μL) were kept at room temperature for 5 min, after which arachidonic acid (30 mM, 20 μL) was added to initiate the reaction. The reaction mixture was incubated for 5 min, following which the absorbance was measured at 570 nm using a UV-visible spectrophotometer. The percentage of COX-2 inhibition was calculated based on the absorbance value per unit of time. Celecoxib served as a positive control for COX-2. The $IC_{50}$ values (in μM) were determined by plotting percentage inhibition *versus* concentration of the sample solution.[37]

**4.2.4. 5-Lipoxygenase inhibitory assay.** The 5-lipoxygenase inhibitory activity of the synthesized derivatives (**10–13** and **15–25**) was carried out using the reported methods.[2] Different concentrations (in the range of 31.25–1000 μg $mL^{-1}$) of the synthesized compounds and 5-lipoxygenase (10 000 U $mL^{-1}$) were used for the assay. Linoleic acid (80 mM) was used as the substrate, while phosphate (50 mM) was used as the buffer with pH 6.3. Mixing of the buffers and the samples and lipoxidase enzyme solution (0.25 mL) was carried out and the mixture was incubated for 5 min. After, linoleic acid (1 mL, 0.6 mM) was added to the mixture. Using a spectrophotometer, the absorbance was measured at a wavelength of 234 nm. The experiment was repeated in triplicate. Zileuton was used as the standard drug. The percent inhibition was calculated using the following equation:

$$\%\text{inhibition} = \frac{\text{abs of control} - \text{abs of control}}{\text{abs of control}} \times 100$$

The $IC_{50}$ values (μM) were determined by plotting inhibition against sample solution concentration.[37]

### 4.3. Methodology for molecular docking

The docking studies were conducted using Molecular Operating Environment (MOE 2016.08). The Protein Data Bank (PDB code 1CX2) was utilized to retrieve the enzyme structures, which were validated through re-docking with their native ligands. Previously reported methods were employed for the preparation of the ligands, downloading the enzymes, energy minimization, 3D protonation, and determination of the binding site.[1,29–33] The Ligand.mdb database of compounds were drawn using the Builder option in MOE. The energy minimization up to 0.01 Gradient was done by using the MMFF94X force field. The MOE window was used to open the enzyme structures. Removal of water molecules (if present) was carried out. The 3D protonation was done for all atoms in the environment at a temperature of 300 K, pH of 7, and salt concentration of 0.1 M. By using the MMFF94X force field, the energy of the complete structure was minimized, followed by docking the compounds in the binding sites of the enzyme. The docking parameters were established for each compound, and ten distinct conformations were generated. The analysis of the lowest binding energy ligand–enzyme complexes was conducted using the MOE ligand interaction module. For the three-dimensional interaction plot, the Discovery Studio Visualizer was employed.[34,38]

### 4.4. Molecular dynamics simulations

A molecular dynamics (MD) simulation was conducted to examine the extensive mobility, stiffness, and sub-cellular functions of proteins. The molecular dynamics simulations were conducted following the docking analysis. The MD simulations were conducted using the online software iMODS.[1] iMODS provides a suitable framework for the analysis of magnified normal modes within their coordinate system. This web server demonstrates flexibility and responsiveness across all major browsers and contemporary devices. It provides information on various parameters, including *B*-factor values, eigenvalue computation, variance, protein structure deformability, elastic network models, and covariance maps.[2,3] The results were obtained within a few minutes by uploading the PDB file of the docked complex to the online server as the input file, while maintaining all parameters at their default settings.[36]

### 4.5. Physicochemical and pharmacokinetic characteristics

SwissADME (https://www.swissadme.ch/) was used to ascertain the physicochemical and pharmacokinetic characteristics of the synthesized derivatives. The thorough evaluation of many pharmacokinetic characteristics, such as absorption, distribution, metabolism, and excretion (ADME), was made easier using this computational method.[7] The bioavailability radar chart algorithms is based on sophisticated statistical and machine learning techniques that have been tested on big molecular datasets with distinct characteristics.[8] Important ADME characteristics were clearly defined within the parameters of the BOILED-Egg model, including passive gastrointestinal absorption (HIA), permeability glycoprotein classification as either substrate or non-substrate, and blood–brain barrier (BBB) penetration.[9]

## Data availability

Data are available from the authors upon request.

## Conflicts of interest

There are no conflicts to declare.

## References

1 R. J. Perry and J. R. Hodges, Attention and executive deficits in Alzheimer's disease: A critical review, *Brain*, 1999, **122**(3), 383–404.
2 K. R. Bales, Interaction of the β-amyloid Protein in Alzheimer's Disease and the Choline Transporter, *Doctoral Dissertation*, Indiana University, 2007.
3 Acetylcholinesterase (AChE) terminates the ACh-mediated neurotransmission and is mostly found in neurons. The therapeutic efficacies of AChE inhibitors in AD have been shown to be due to augment synaptic ACh levels in the cerebral cortex and improve cholinergic transmissions.
4 T. H. Ferreira-Vieira, I. M Guimaraes, F. R Silva and F. M Ribeiro, Alzheimer's disease: targeting the cholinergic system, *Curr. Neuropharmacol.*, 2016, **14**(1), 101–115.
5 G. T. Grossberg, Cholinesterase inhibitors for the treatment of Alzheimer's disease:: getting on and staying on, *Curr. Ther. Res.*, 2003, **64**(4), 216–235.
6 C. G. Ballard, N. H. Greig, A. L. Guillozet-Bongaarts, A. Enz and S. Darvesh, Cholinesterases: roles in the brain during health and disease, *Curr. Alzheimer Res.*, 2005, **2**(3), 307–318.
7 L. Pezzementi, F. Nachon and A. Chatonnet, Evolution of acetylcholinesterase and butyrylcholinesterase in the vertebrates: an atypical butyrylcholinesterase from the Medaka Oryzias latipes, *PLoS One*, 2011, **6**(2), e17396.
8 A. S. Kalgutkar, N. Castagnoli Jr and B. Testa, Selective inhibitors of monoamine oxidase (MAO-A and MAO-B) as probes of its catalytic site and mechanism, *Med. Res. Rev.*, 1995, **15**(4), 325–388.
9 M. G. Erkkinen, M. O. Kim and M. D. Geschwind, Clinical neurology and epidemiology of the major neurodegenerative diseases, *Cold Spring Harbor Perspect. Biol.*, 2018, **10**(4), a033118.
10 L. Minghetti, Cyclooxygenase-2 (COX-2) in inflammatory and degenerative brain diseases, *J. Neuropathol. Exp. Neurol.*, 2004, **63**(9), 901–910.
11 P. S. Khansari and L. Coyne, NSAIDs in the treatment and/or prevention of neurological disorders, *Inflammopharmacology*, 2012, **20**(3), 159–167.
12 M. Yan, S. Zhang, C. Li, Y. Liu, J. Zhao, Y. Wang and L. Zhang, 5-Lipoxygenase as an emerging target against age-related brain disorders, *Ageing Res. Rev.*, 2021, **69**, 101359.
13 T. A. E. R. Farghaly, M. A. Abdallah and H. K. MMAHMOUD, Synthesis of novel 1, 2, 4-triazoles and triazolo-thiadiazines as anticancer agents, *Turk. J. Chem.*, 2015, **39**(5), 955–969.
14 Z. A. Kaplancıklı, G. Turan-Zitouni, A. Özdemir and G. Revial, New triazole and triazolothiadiazine derivatives as possible antimicrobial agents, *Eur. J. Med. Chem.*, 2008, **43**(1), 155–159.
15 I. Khan, A. Ibrar, S. Zaib, S. Ahmad, N. Furtmann, S. Hameed and J. Iqbal, Active compounds from a diverse library of triazolothiadiazole and triazolothiadiazine scaffolds: Synthesis, crystal structure determination, cytotoxicity, cholinesterase inhibitory activity, and binding mode analysis, *Bioorg. Med. Chem.*, 2014, **22**(21), 6163–6173.
16 I. Khan, A. Ibrar and N. Abbas, Triazolothiadiazoles and triazolothiadiazines–Biologically attractive scaffolds, *Eur. J. Med. Chem.*, 2013, **63**, 854–868.
17 I. Khan, *et al.*, Exploration of a library of triazolothiadiazole and triazolothiadiazine compounds as a highly potent and selective family of cholinesterase and monoamine oxidase inhibitors: design, synthesis, X-ray diffraction analysis and molecular docking studies, *RSC Adv.*, 2015, **5**(27), 21249–21267.
18 S. M. A. Abid, S. Aslam, S. Zaib, S. M. Bakht, M. Ahmad, M. M. Athar, J. M. Gardiner and J. Iqbal, Pyrazolobenzothiazine-based carbothioamides as new structural leads for the inhibition of monoamine oxidases: design, synthesis, in vitro bioevaluation and molecular docking studies, *Medchemcomm*, 2017, **8**(2), 452–464.
19 I. Khan, *et al.*, Active compounds from a diverse library of triazolothiadiazole and triazolothiadiazine scaffolds: Synthesis, crystal structure determination, cytotoxicity, cholinesterase inhibitory activity, and binding mode analysis, *Bioorg. Med. Chem.*, 2014, **22**(21), 6163–6173.
20 R. K. P. Tripathi and S. R. Ayyannan, Monoamine oxidase-B inhibitors as potential neurotherapeutic agents: An overview and update, *Med. Res. Rev.*, 2019, **39**(5), 1603–1706.
21 U. M. Zahid, A. S. Sohail, A. Mohammed, I. Hasher, R. Sanwa, S. A. Shakir and A. Mumtaz, An extensive experimental and DFT studies on highly selective detection of nitrobenzene through deferasirox based new fluorescent sensor, *Spectrochim. Acta, Part A*, 2024, **306**, 123607.
22 S. Alcaro, M. L. Bolognesi, A. T. García-Sosa and S. Rapposelli, Multi-target-directed ligands (MTDL) as challenging research tools in drug discovery: From design to pharmacological evaluation, *Front. Chem.*, 2019, **7**, 71.

23 (*a*) M. Mahmood, *et al.*, Evaluation of 3,4-diethoxy substituted thioureas and their thiazole derivatives as potent anti-Alzheimer's agents: Synthesis, DFT, biological activity and molecular modeling investigations, *J. Mol. Struct.*, 2024, **1314**, 138760; (*b*) M. Rudrapal, *et al.*, Dual synergistic inhibition of COX and LOX by potential chemicals from Indian daily spices investigated through detailed computational studies, *Sci. Rep.*, 2023, **13**(1), 8656.

24 F. A. Larik, *et al.*, New cholinesterase inhibitors for Alzheimer's disease: Structure activity relationship, kinetics and molecular docking studies of 1–butanoyl–3–arylthiourea derivatives, *Int. J. Biol. Macromol.*, 2018, **116**, 144–150.

25 S. Rauhamäki, *et al.*, Structure-Activity Relationship Analysis of 3-Phenylcoumarin-Based Monoamine Oxidase B Inhibitors, *Front. Chem.*, 2018, **6**, DOI: **10.3389/fchem.2018.00041**.

26 C. Almansa, *et al.*, Synthesis and Structure−Activity Relationship of a New Series of COX-2 Selective Inhibitors: 1,5-Diarylimidazoles, *J. Med. Chem.*, 2003, **46**(16), 3463–3475.

27 *MOE (Molecular Operating Environment) Version 2016.01*, Chemical Computing Group, (CCG), **https://www.chemcomp.com/MOE/Molecular_Operating_Environment.htm**.

28 J. R. López-Blanco, J. I. Aliaga, E. S. Quintana-Ortí and P. Chacón, iMODS: Internal coordinates normal mode analysis server, *Nucleic Acids Res.*, 2014, **42**, W271–W276.

29 J. R. López-Blanco, J. I. Garzón and P. Chacón, iMod: multipurpose normal mode analysis in internal coordinates, *Bioinformatics*, 2011, **27**(20), 2843–2850.

30 J. Kovacs, P. Chacón and R. Abagyan, Predictions of Protein Flexibility: First Order Measures, *Proteins:Struct., Funct., Bioinf.*, 2004, **56**(4), 661–668.

31 A. Daina and V. Zoete, Application of the SwissDrugDesign online resources in virtual screening, *Int. J. Mol. Sci.*, 2019, **20**(18), 4612.

32 C.-Y. Jia, *et al.*, A drug-likeness toolbox facilitates ADMET study in drug discovery, *Drug discovery today*, 2020, **25**(1), 248–258.

33 C. A. Lipinski, *et al.*, Experimental and computational approaches to estimate solubility and permeability in drug discovery and development settings, *Adv. Drug Delivery Rev.*, 1997, **23**(1–3), 3–25.

34 A. Daina, O. Michielin and V. Zoete, SwissADME: a free web tool to evaluate pharmacokinetics, drug-likeness and medicinal chemistry friendliness of small molecules, *Sci. Rep.*, 2017, **7**(1), 42717.

35 G. L. Ellman, *et al.*, A new and rapid colorimetric determination of acetylcholinesterase activity, *Biochem. Pharmacol.*, 1961, **7**(2), 88–95.

36 S. U. Qazi, *et al.*, Semicarbazones, thiosemicarbazone, thiazole and oxazole analogues as monoamine oxidase inhibitors: Synthesis, characterization, biological evaluation, molecular docking, and kinetic studies, *Bioorg. Chem.*, 2021, **115**, 105209.

37 M. Mahmood, Z. Hussain, M. Z. Ullah, S. A. Ejaz, A. Fayyaz, U. Rashid, J. Iqbal and A. Mumtaz, Evaluation of 3,4-diethoxy substituted Thioureas and Their Thiazole Derivatives as Potent anti-Alzheimer's agents: Synthesis, DFT, Biological Activity and Molecular Modeling Investigations, *J. Mol. Struct.*, 2024, **1314**, 138760.

38 A. Munir, A. Khushal, K. Saeed, A. Sadiq, R. Ullah, G. Ali, Z. Ashraf, E. U. Mughal, M. Saeed Jan, U. Rashid and I. Hussain, Amara Mumtaz Synthesis, in-vitro, in-vivo anti-inflammatory activities and molecular docking studies of acyl and salicylic acid hydrazide derivatives, *Bioorg. Chem.*, 2020, **104**, 104168.